Research Article

Development and Assessment of the Sand Dust Prediction Model by Utilizing Microwave-Based Satellite Soil Moisture and Reanalysis Datasets in East Asian Desert Areas

Hyunglok Kim,[1] Muhammad Zohaib,[1] Eunsang Cho,[2] Yann H. Kerr,[3] and Minha Choi[1]

[1]*Water Resources and Remote Sensing Laboratory, Graduate School of Water Resources, Sungkyunkwan University, Suwon, Gyeonggi-do 440-746, Republic of Korea*
[2]*Department of Civil and Environmental Engineering, University of New Hampshire, Durham, NH, USA*
[3]*Centre d'Etudes Spatiales de la BIOsphère (CESBIO), CNES, CNRS, IRD, UPS, Toulouse, France*

Correspondence should be addressed to Minha Choi; mhchoi@skku.edu

For several decades, satellite-based microwave sensors have provided valuable soil moisture monitoring in various surface conditions. We have first developed a modeled aerosol optical depth (AOD) dataset by utilizing Soil Moisture and Ocean Salinity (SMOS), Advanced Microwave Scanning Radiometer 2 (AMSR2), and the Global Land Data Assimilation System (GLDAS) soil moisture datasets in order to estimate dust outbreaks over desert areas of East Asia. Moderate Resolution Imaging Spectroradiometer- (MODIS-) based AOD products were used as reference datasets to validate the modeled AOD (MA). The SMOS-based MA (SMOS-MA) dataset showed good correspondence with observed AOD (*R*-value: 0.56) compared to AMSR2- and GLDAS-based MA datasets, and it overestimated AOD compared to observed AOD. The AMSR2-based MA dataset was found to underestimate AOD, and it showed a relatively low *R*-value (0.35) with respect to observed AOD. Furthermore, SMOS-MA products were able to simulate the short-term AOD trends, having a high *R*-value (0.65). The results of this study may allow us to acknowledge the utilization of microwave-based soil moisture datasets for investigation of near-real time dust outbreak predictions and short-term dust outbreak trend analysis.

1. Introduction

Mineral dust plays a critical role in climate forcing and in the atmospheric radiation budget by scattering, absorbing, and reemitting longwave and shortwave radiation [1–4]. Mineral dust modifies the microphysical and optical properties of clouds, thereby indirectly affecting climate [5, 6]. It also supplies nutrient transfer to oceans and terrestrial ecosystems and neutralizes acid precipitation [7–9]. However, dust storms can also harm human lives by negatively affecting public health, the solar economy, agriculture, and transportation [10, 11]. The Korean peninsula and Japan are located to the east of China and are annually damaged by the Asian dust storms, called "Hwangsa" in Korean and "Kosa" in Japanese. These dust storms are mostly generated from deserts in Northern China, such as the Taklimakan and Gobi Deserts. The dust then blows into neighboring nations on the westerlies during the spring season from March to May [12]. Hwangsa can cause severe cardiovascular and respiratory diseases [13, 14]. Moreover, the frequency of dust events has been steadily increasing annually in Eastern Asia [15, 16]. Therefore, the ability to identify dust sources and to detect dust events is essential to predict dust outbreaks precisely in response to climate change and to plan prevention measures against dust disasters.

The mechanism through which dust is emitted should be further clarified in order to quantitatively understand and predict dust outbreaks. Many factors determine the mobilization of sand in dust source regions, including erosivity factors (i.e., strong wind speed) and erodibility factors (e.g., soil properties, soil moisture, and type of land cover). Many of the mineral dust source regions in East Asia are located in

large bare deserts, and therefore, the surface wind speed and soil moisture (SM) are considered to be the primary factors that control interannual variation in the frequency of dust outbreaks [15, 17]. Various studies were previously conducted using wind tunnel experiments in laboratories or in fields to examine the effect of SM on wind erosion [18–23]. However, most of these studies were not able to fully reflect large-scale dust outbreak phenomena under natural conditions. In order to overcome this challenge, the synergetic use of remote sensing datasets and global assimilated datasets is invaluable. This enables global-scale dust emission studies to be conducted beyond observatory-scale dust research [24, 25].

In recent years, many efforts have been made to identify dust source regions and to detect dust events based on satellite remote sensing techniques [10, 26–34]. However, the previous studies hardly explain the conditions in the dust source regions that produce dust outbreaks because most analyses are based on data obtained from visible and infrared sensed datasets which have limitations under cloudy and dusty weather conditions. Thus, this study investigates dust outbreak phenomena using microwave-based satellite remote sensing techniques to estimate the surface conditions (i.e., surface SM) when dust events occur. Several studies have investigated surface SM from satellite-based microwave instruments [35–39]. Satellite-based SM measurements were required during the initial states of weather forecasting and climate modeling over vast scales [40–43]. Recently, satellite missions specializing in global SM measurements have been conducted. The National Aeronautics and Space Administration's (NASA) Delta II rocket was launched in January 2015 carrying the Soil Moisture Active Passive (SMAP) to monitor SM and to detect the frozen or thawed state of soils [39]. Many other promising satellites have been launched to acquire global SM contents, such as the Advanced Scatterometer (ASCAT), Advanced Microwave Scanning Radiometer 2 (AMSR2), and Fengyun [40–48]. Of these, certain satellites have shown better performance in determining the SM products in specific regions because of their specific characteristics, such as the sensor type (e.g., active and passive), platform overpass time, band frequency, polarization, retrieval algorithm, and calibration systems [42, 49, 50].

The Soil Moisture and Ocean Salinity (SMOS) was launched by the European Space Agency (ESA) and the Centre National d'Etudes Spatiales (CNES) of France in November 2009 as the second Earth Explorer opportunity mission [36, 38]. As the name implies, SMOS has been particularly designed to provide global SM observations using the L-band, an optimal wavelength for retrieving SM from space [36, 38]. In particular, SMOS-derived SM contents have proven to be advantageous in desert areas because the L-band signal exhibits a distinct behavior over extremely dry surface conditions [42, 50, 51]; as such, it is hardly influenced by polluted atmospheric conditions [36]. Hence, SMOS measurements have the potential for use in mineral dust research over desert regions. However, no such research has been conducted to date.

The AMSR2, a follow-up microwave sensor to the AMSR for Earth Observing System (AMSR-E), is a passive microwave instrument that has been providing global near-surface SM data since its launch in May 2012. The AMSR2 SM product has been widely validated by many studies [41, 52, 53].

The present study uses SMOS- and AMSR2-derived SM measurements and the Global Land Assimilation Dataset System (GLDAS) to investigate dust outbreaks over the desert regions of East Asia. The relationships among the SM, wind speed, and aerosol optical depth (AOD) are utilized to estimate dust outbreak phenomena. The main objectives of this study are (1) to estimate the modeled AOD (hereafter MA) datasets based on different SM and GLDAS wind speed datasets, (2) to validate MAs with the observed MODIS-AOD products and short-term trend analysis, and (3) to analyze the spatial distribution of MA products and observed AOD datasets in different seasons. To the best of our knowledge, this study is the first to use SMOS and AMSR2 products to predict dust outbreaks at the global-scale.

2. Datasets and Study Areas

In this study, the erosivity factor (i.e., wind speed), erodibility factors (i.e., soil properties, sand fractions, and SM), surface conditions (i.e., surface temperature), and precipitation were considered in order to analyze the effect of SM on dust outbreaks over deserts in East Asia.

The US Department of Agriculture (USDA) topsoil texture classification was used with the Harmonized World Soil Database (HWSD) to define the desert regions and to obtain information on the land and the atmosphere over the land. The SM contents were retrieved from SMOS and AMSR2; SM, wind speed (WS), surface temperature, and precipitation datasets from GLDAS were utilized for generating MA products. Atmospheric properties were obtained using the Moderate Resolution Imaging Spectroradiometer (MODIS) sensors on the Aqua satellite (Refer to the following sections for further details regarding those datasets). All of the datasets were gathered during 2015 and were resampled to a spatial resolution of $0.25° \times 0.25°$.

2.1. Land Cover and Land Properties Dataset. Land cover and land properties datasets are used in this study to identify dust source regions and investigate dust outbreak conditions. The land cover dataset is obtained from Biosphere Atmosphere Transfer Scheme (BATS). BATS landform categories were created by Dickinson et al. [54] and modified by Olson [55] to support land-atmosphere modeling. Similarly, the land properties dataset is obtained from the Harmonized World Soil Database (HWSD), which is a raster database that contains more than 16,000 different soil mapping units at a spatial resolution of $1\,km \times 1\,km$. This database combines regional and national updates of soil information worldwide. It consists of 221 million grid cells and is contained within the 1 : 5,000,000 scale FAO-UNESCO Soil Map of the World. In particular, the HWSD has been applied in dust research to identify dust sources and investigate dust outbreak conditions

[1] Taklimakan Desert   [5] Hunshandake Desert
[2] Gurbantunggut Desert   [6] Horqin Desert
[3] Kumtag and Qaidam Basin Desert   [7] Gobi Desert
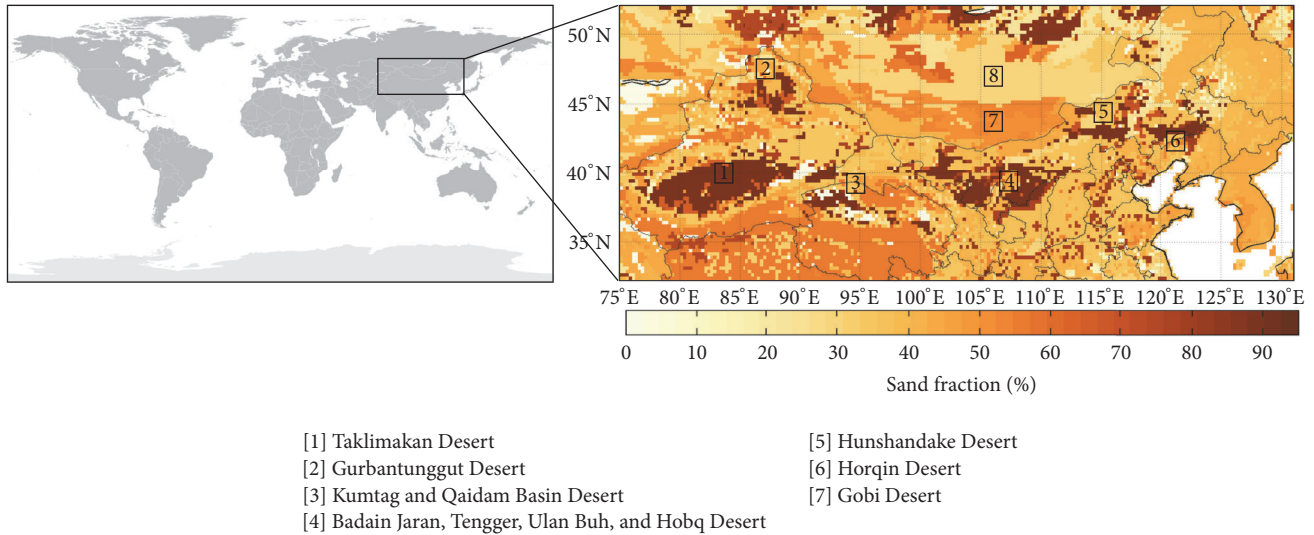[4] Badain Jaran, Tengger, Ulan Buh, and Hobq Desert

Figure 1: The East Asia sand fractions were retrieved according to the Harmonized World Soil Database (HWSD). All of the identified desert regions were recognized as the most famous dust sources around the world. Well-known desert regions (#1 to #6) are classified as sand by the USDA classification and exhibit a sand fraction that is greater than 80%.

as well as in several other research fields [56–59]. The study area was masked based on the BATS desert land cover class and an HWSD sand fraction greater than 80% to define the desert regions.

2.2. Study Areas. Figure 1 shows the spatial description of the study areas in terms of the sand fraction. Boxes 1 to 7 show the famous desert areas that have been regarded as the major mineral dust source regions in East Asia [12, 15, 60–62]. In this study, these bare desert areas have been classified using HWSD sand fractions greater than 80% and desert regions from the BATS model. Through this masking process, all major deserts in East Asia except the Gobi Desert were extracted. About 1,012,500 km^2 (1,620 pixels) have been identified as desert areas, and the average sand, clay, and silt fractions were 87.6, 5.7, and 7.0% respectively. In these regions, especially during spring, frequent dust outbreaks result in Asian dust storms in neighboring countries [63, 64].

2.3. SMOS for Soil Moisture Contents. SMOS provides global near-surface SM (SSM) and covers the globe in three days, with a ground resolution ranging from 27 to 55 km (the average spatial resolution is 43 km), and its mission is to retrieve SSM at an accuracy of 0.04 m^3/m^3 at a depth of 3 to 5 cm. SMOS has been particularly designed to be on a sun-synchronous orbit, ascending in the morning at 0600 local time (LT) and descending at 1800 LT [36–38]. The SMOS instrument is an L-band (1.41 GHz, λ = 21 cm) 2D interferometer radiometer that is considered to have the most suitable frequency for SM retrieval. In particular, the L-band frequency offers the added advantage of taking measurements in all weather conditions [36, 65]. In addition, radiometers are expected to perform better than scatterometers in dry areas [49, 50, 66, 67]. However, the L-band is negatively impacted

by radio frequency interference (RFI) from illegal emissions in the protected passive band and unwanted emissions from active services operating in neighboring bands. Thus, several studies have been conducted since the SMOS mission began to mitigate the effects of RFI contamination [68]. The daily SSM products (L3) that were considered in this study were provided by the Centre Aval de Traitement des Données (CATDS Centre) with a spatial sampling of 25 km × 25 km in NetCDF format. We calculated the preceding one- to five-day composite SM products (ascending). This past-compositing SM process is considered because the antecedent moisture conditions that are detected by the SMOS may have the capability to predict dust outbreaks in the near future. Additionally, the FL_RAIN science flag is used for filtering the heavy rainfall events.

2.4. AMSR2 for Soil Moisture Contents. The Japan Aerospace Exploration Agency (JAXA), with the cooperation of NASA, launched AMSR2 sensor on board the Global Change Observation Mission 1-Water (GCOM-W1) platform in May 2012. It is the successor to JAXA's AMSR-E on board NASA's Aqua satellite. It utilizes microwave frequencies at C1- (6.9 GHz), C2- (7.3 GHz), and X- (10.65 GHz) bands for SM measurements and provides a 1,450 km swath width and 25 km spatial resolution associated with a revisit time of one to two days. The AMSR2 crosses the equator at 01:30 LT and 13:30 LT for descending and ascending orbits, respectively. Primarily, two algorithms are used to derive AMSR2-based SM products from measured brightness temperature: JAXA and NASA-VUA (VU University Amsterdam) Land Parameter Retrieval Model (LPRM) products [46]. Originally, both of these algorithms utilized a simple radiative transfer model [69]. Moreover, LPRM provides AMSR2 SM retrievals for both C- and X-band microwave frequencies, whereas the

JAXA algorithm provides SM retrievals only for the X-band. The LPRM algorithm, however, is expected to be more accurate, which enables the retrievals of the SM and vegetation optical depth, simultaneously, from horizontal and vertical polarized T_b measurements [70]. The AMSR2 SM products used in this study were cross-validated with the AMSR-E slow rotation dataset (http://global.jaxa.jp/press/2015/12/20151207_amsr-e.html). In this study, we only utilized the LPRM X-band SM dataset for conciseness, because SM from the C1- and C2-bands showed almost the same temporal patterns as the SM from the X-band over the study area.

2.5. MODIS for Atmosphere Products. The dust outbreak states that are characterized by the AOD and Angstrom exponent (AE) values were used in this study and were collected by the MODIS platform aboard NASA's Earth Observing System- (EOS-) Terra and Aqua polar orbiter satellites. Aqua was launched on May 4, 2002, into a sun-synchronous orbit with an ascending orbit at 1330 LT and a descending orbit at 0130 LT. The Naval Research Laboratory (NRL) receives the global digital data from Aqua in near-real time. The MODIS data are distributed by NASA's Goddard Earth Sciences Data and Information Services Centre (GES DISC) and are provided not only for the atmosphere but also for the land, cryosphere, and oceans [71, 72].

The MODIS sensor has 36 narrow spectral bands and measures in the 0.4–14.4 μm range. Specific channels, including visible and infrared bands (e.g., bands 1, 2, 3, 4, 26, 31, and 32), have been effectively used to detect mineral particles [30, 32, 34]. In particular, deep blue products (deep blue uses information from blue channels such as bands 3 and 8) are generally used over bright land surfaces to detect mineral dust. Deep blue was developed because the standard MODIS aerosol LAND measurements could not be used to retrieve data over bright surfaces, such as desert areas. For more details on the deep blue algorithm, refer to Hsu et al. [33]. In this study, the MYD04_L2 Aqua deep blue AOD (hereafter, MODIS-AOD) and AE datasets (550 nm) were employed because these datasets have already been extensively validated and have been successfully utilized in several studies [10, 25, 29, 30, 73, 74]. To ensure consistency in the analyses, the MODIS-AOD products were upscaled to 0.25°.

2.6. GLDAS for Land Surface Products. GLDAS is a result of datasets assimilated through cooperation of the National Centres for Environmental Prediction (NCEP), NASA, the National Oceanic and Atmosphere Administration (NOAA), and the Goddard Space Flight Centre (GSFC). GLDAS is a global-scale assimilation and modeling system that has been developed using several satellite- and ground-based datasets to provide the best estimation of the land surface conditions in near-real time [75–77]. The analyses were based on the GLDAS/Noah products because these provide various land surface products with a high spatial resolution (0.25°) for every 3-hour period. In this study, WS (m/s, height of 10.0 m), soil temperature (K, depth of 0–10.0 cm), and precipitation (mm/3 h) products were also obtained from GLDAS. These

products have been extensively used in hydrometeorological applications and validation studies [45, 78, 79].

3. Methodology

The SMOS, AMSR2, and MODIS overpass datasets are available at local times, whereas the GLDAS/Noah products are based on the Universal Time Coordinate (UTC) system. It is of utmost importance that the UTC time of GLDAS products must match the satellite local overpass time before they are used for dust outbreak prediction. The SMOS overpass time (ascending, 0600 LT) precedes the MODIS and AMSR2 overpass time (ascending, 1330 LT). AOD from MODIS, which detects the dust outbreak state, is assumed as the reference dataset in this study, whereas SMOS and AMSR2 which retrieved SM are used alongside the GLDAS wind speed product to obtain the modeled AOD. The SMOS overpasses the study areas from 2100 to 0100 UTC (0600 LT, ascending), and MODIS overpasses the study areas from 0430 to 0830 UTC (1330 LT, ascending). Theoretically, the overpass times have a lag of about 7.5 h for SMOS-based AOD prediction (Figure 2(a)). GLDAS products are available at 3-hour intervals (0000, 0300, 0600, 0900, 1200, 1500, 1800, and 2100 UTC). Because the study area has five different time zones, we matched the local time with the UTC for GLDAS products. Considering the SMOS and AMSR2-based dust model for zones 1 and 2, GLDAS products at 0000 UTC and 0300 UTC were used. For zones 3, 4, and 5, however, GLDAS products at 2100 UTC of the previous day and 0600 UTC of the same day were used (Figure 2(b)). Furthermore, fine mode aerosols, such as transported dust and biomass burning aerosols, were eliminated by setting an AE threshold greater than 0.35 [10, 24, 80].

3.1. Developing Modeled AOD Products from Satellites-Based SM and GLDAS Dataset. In this study, due to the shorter period of data availability, we assumed that SMOS-based and AMSR2-based SM retrievals have a negative relationship with AOD, as previously proposed by Kim and Choi [24] (Figure 3). Since AMSR2 and SMOS datasets are only available every four years and seven years, respectively, deriving the same number of equations as in the study by Kim and Choi [24] was not possible. Their study utilized an 11-year dataset (containing 27.261 million data points), which provided sufficient information to make feasible assumptions regarding the derived equations [24].

The WS magnitude is divided into 10 groups (3 to 12 m/s of WS) at 1 m/s intervals, as in Kim and Choi [24]. Alternatively, WS lower than 4 m/s were classified as 3 m/s, and WS higher than 12 m/s were classified as 12 m/s. Figure 3 shows the previous research finding that, generally, the averaged-AOD values decreased exponentially according to the various conditions of the WS and SM contents [24]. The exponential decrease in the averaged-AOD patterns with the increase in SM and decrease in WS is similar to trends presented in prior studies. The physical meaning of the patterns in Figure 3 is that a stronger WS (i.e., 6.5 m/s) is required to generate dust events under wet soil conditions because highly moistened
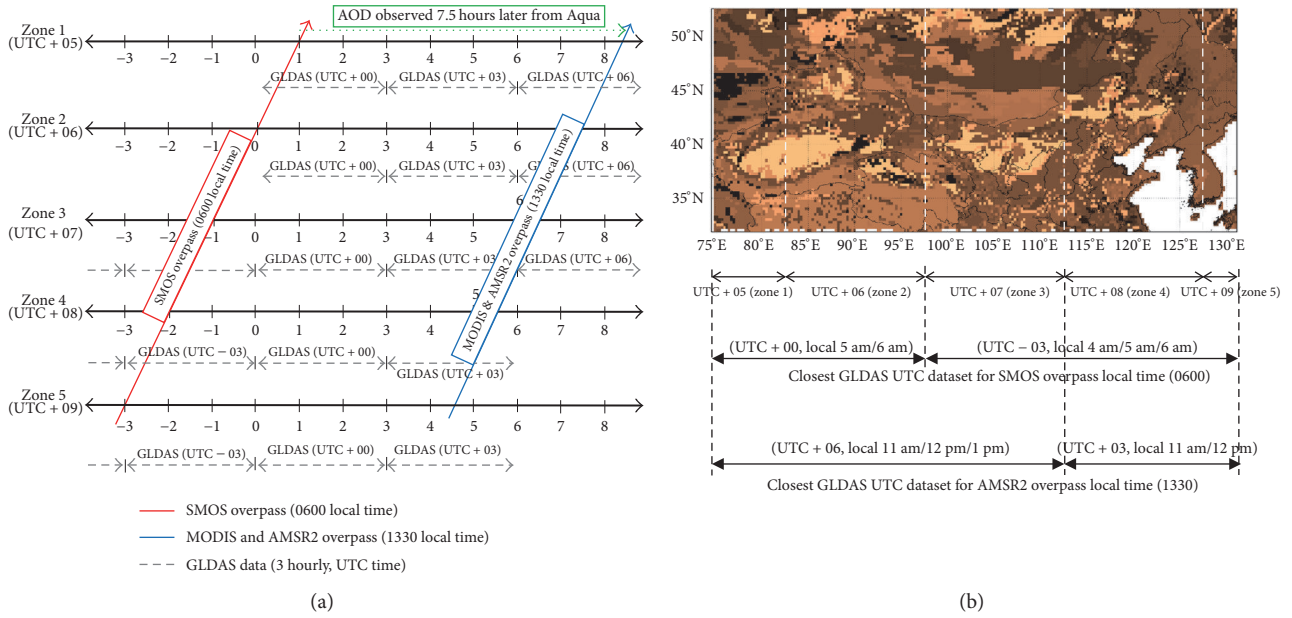
(a)

(b)

FIGURE 2: A graphical representation of the methodology for matching GLDAS UTC zone based products with local overpass times of SMOS, AMSR2, and MODIS in different time zones within the study area.
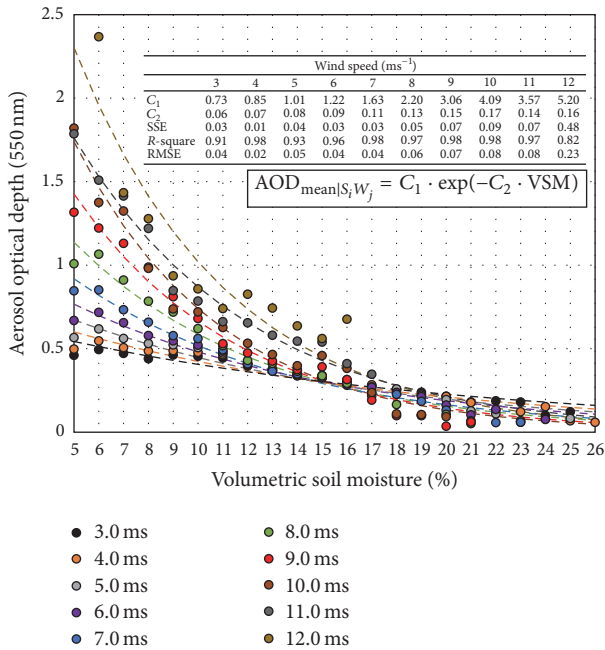

FIGURE 3: The relationship between average AOD and volumetric soil moisture under different wind speed conditions. The uppermost curves on the graph represent the strongest wind speed conditions. Constants (C_1 and C_2) and statistical information for each curve are included [24].

sand particles have a more sturdy and cohesive strength among soil particles [81, 82]. Thus, a stronger WS and drier surface conditions have a greater propensity to produce dusty atmospheric conditions. Furthermore, the AOD value may be almost unaffected by the SM dynamics in a weaker WS or in

damped conditions (about 16% of the SM). Moreover, under a stronger WS (higher than 6.0 m/s) and drier land surface conditions (less than about 16% of the volumetric SM), SM plays an important role in dust outbreak processes.

Considering the equation in Figure 3, the AOD values could be estimated using the following equation with different constants for C_1 and C_2 that are contingent on the magnitude of WS:

$$\text{Modeled\_AOD}_i = C_1 \times \exp\left(-C_2 \times \text{SM}_i\right). \tag{1}$$

From (1), we can establish an MA by using SM (%) and WS (m/s) datasets. In this study, we considered four different MAs: the SMOS SM and GLDAS WS-based MA (hereafter, SMOS-MA), the AMSR2 SM and GLDAS WS-based MA (hereafter, AMSR2-MA), the MA based on GLDAS dataset at 0600 (hereafter, GLDAS-MA_6), and the MA based on GLDAS dataset at 1200 (hereafter, GLDAS MA_12). The GLDAS-MA_6 and GLDAS-MA_12 enable us to make a fair comparison between satellite and GLDAS SM products for their dust outbreak prediction.

3.2. Soil Moisture Composition and Moving Average of MA Products.
We used five different composite SM products (composited day: one- to five-day) to investigate the impact of antecedent SM on dust outbreaks. We composited SMOS, AMSR2, and GLDAS SM using following equation:

$$\text{composited SM}_{\text{doy}} = \frac{\sum_{i=\text{doy}-\text{comp\_day}}^{\text{doy}} \text{SM}_i}{\text{comp\_day}}, \tag{2}$$

where doy is day of year.

To calculate the time series of the MA dataset of the desert regions, we consolidated the daily available MA data

over the desert regions and averaged them by using following equation:

$$\text{average } MA_{\text{doy}} = \frac{\sum_{i=1}^{N} MA_{i,\text{doy}}}{N}, \tag{3}$$

where N is the number of available MA data over the desert pixels at doy and doy is day of year.

We set the composited day from one to five days. Moreover, the 11-day moving averaged MA was calculated as follows:

$$\text{moving averaged } MA_{\text{doy}} = \frac{\sum_{i=\text{doy}-5}^{\text{doy}+5} MA_i}{11}. \tag{4}$$

3.3. Comparison Metrics. The Pearson correlation coefficient (R) between MA and MODIS-AOD was calculated using (5). The bias (see (6)) was also considered. All metrics were used when the p value was less than 0.05:

$$R = \sqrt{1 - \frac{\sum (MA - MODIS\text{-}AOD)^2}{\sum \left(MA - \overline{MODIS\text{-}AOD}\right)^2}} \tag{5}$$

$$\text{Bias} = \text{mean} (MODIS\text{-}AOD - MA). \tag{6}$$

4. Results and Discussion

In East Asian deserts, dust outbreaks usually occur from early March to late May. Figure 4(h) shows the time series for the MODIS-AOD satellite data in 2015. The seasonal patterns of dust outbreaks are consistent with the results of previous research [12, 16]. The patterns can be well accounted for by simultaneously considering the temporal changes of SM and WS conditions (Figures 4(b) and 4(d)). The MODIS-AOD values (Figure 4(h)) were usually high under low SM and high WS conditions. However, this is not easily explained because the threshold value of WS at which dust outbreaks occur is greatly influenced by the SM conditions over the source areas [81–84]. Moreover, the threshold values for WS and SM shifted according to the AOD setting for dust outbreak states [24].

4.1. Validation of MAs with AOD Observations. Validation of the MAs with an assumed reference dataset from the MODIS-AOD was performed to check the reliability of the models for future prediction. Figure 5 shows the temporal pattern of the MODIS-AOD and different MAs in the desert regions of East Asia for 2015. A temporal comparison between the SMOS-MA and MODIS-AOD shows a good correlation (R-value: 0.56), but mostly higher than MODIS-AOD (Figure 5(a)). In the case of the AMSR-MA, a low correlation coefficient indicates that the temporal pattern of the MA dataset does not follow the reference AOD well, as compared to the SMOS-MA, and has an overall negative bias demonstrating that it usually underestimates the AOD with respect to the MODIS-AOD (Figure 5(b)). When the MA is based on the GLDAS SM product matched with the SMOS (i.e., the GLDAS-MA_6) and AMSR2 (i.e., the GLDAS-MA_12)

overpass LT, the correlation coefficient is still lower than the SMOS-MA and underestimates the AOD; however, both of the GLDAS-based models showed very similar temporal patterns (Figure 5(c)). The analysis was further extended to evaluate the prediction based on one- to five-day composite SM products to consider the effect of antecedent conditions for all MAs (Table in Figure 5). The results indicate that different antecedent soil moisture conditions do not have much influence on dust outbreaks, which can be explained by the moisture memory concept [85, 86]. Specifically, desert regions have persistently very low SM conditions without dramatic daily fluctuations; thus, the WS, which is the major factor in bringing about dust outbreaks in bare desert areas, would affect more the timing of dust outbreaks. This conclusion is supported by the time series results shown on Figures 4(b) and 4(d). However, additional studies should be conducted that simultaneously consider the specific amount of variability of the antecedent WS and SM conditions before a dust outbreak event. Investigating these aspects is beyond the scope of this study.

4.2. Short-Term AOD Trends Analysis. In Figure 6, the 11-day moving average MA products are depicted using (3) for the short-term dust trends analysis. The solid red, light blue, orange, gray, and purple lines indicate moving averages of the MODIS-AOD, SMOS-MA, AMSR2-MA, GLDAS-MA_6, and GLDAS-MA_12, respectively. The table in Figure 6 includes the statistical results of each MA, including correlation and bias values, by comparing them with moving averaged AOD from MODIS-AOD. The SMOS-MA products showed the best R-value (0.65) among other MAs. However, it showed a reversed trend and overestimated AOD notably in the fall season. This might be explained by unforeseen rainfall events that were not been considered during the 7.5 h time interval between the overpass time of SMOS and MODIS (Figure 2). Particularly, in East Asia, these regions experience monsoon season from September to October; thus, aerosols in the atmosphere might suddenly decrease because of frequent rainfall events. These abrupt AOD abatements would have not been predicted based on the previous information of SM and WS. During the spring and the summer seasons, SMOS better simulated AOD trends, with an R-value of 0.70. Similarly, the GLDAS-MA_12 showed an R-value of 0.62, but the GLDAS-MA_12 also presented reversed AOD trends similar to the SMOS-MA. The AMSR2-MA and the GLDAS-MA_6 products exhibited R-values of 0.46 and 0.45, respectively, and underestimated AOD in the spring and the summer seasons and overestimated AOD in the fall season.

4.3. Limitations and Advantages of MA Products. Figures 7(a), 7(b), and 7(c) depict exemplary maps of the SMOS-MA, masked MODIS-AOD dataset (i.e., eliminating AOD values when AE > 0.35), and original AOD measurements from MODIS-AOD (without AE masking) for investigating a feature of MA products. Box (a)-1 predicts AOD to be between 0.3 and 2.5 in the box area; however, box (b)-1 and box (c)-1 do not show any aerosol observations. There are two feasible reasons that might support this mismatch.
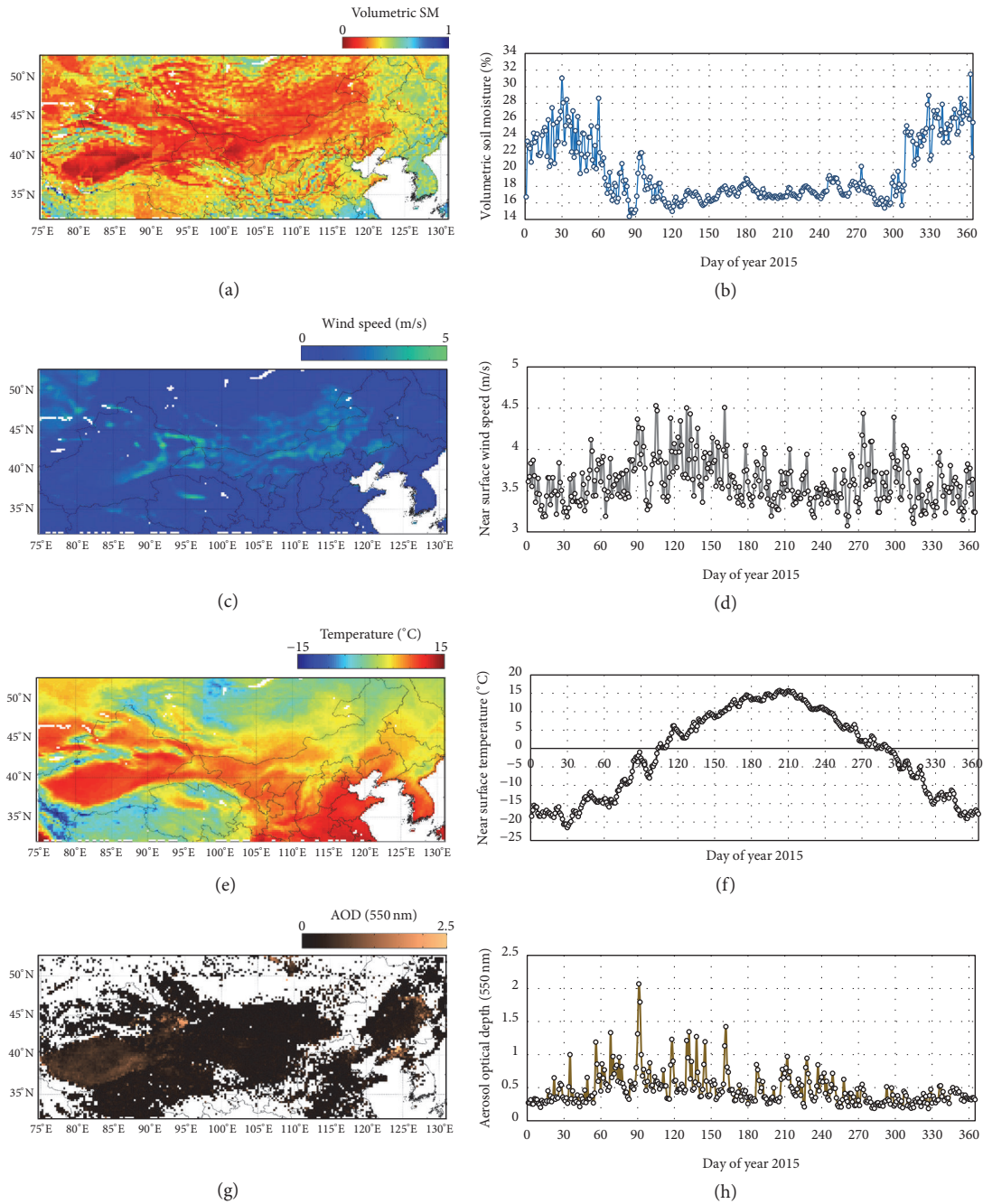
(a)

(b)

(c)

(d)

(e)

(f)

(g)

(h)

FIGURE 4: (a) The map of GLDAS volumetric soil moisture contents (%). (b) The time series for the average value of volumetric soil moisture from the GLDAS for the desert regions. (c) The map of GLDAS near-surface wind speed (m/s). (d) The time series for the average value of the GLADS near-surface wind speed for the desert regions. (e) The map of GLDAS near-surface temperature (°C). (f) The time series for the average value of near-surface temperature for the desert regions. (g) The map of MODIS-based aerosol optical depth (AOD). (h) The time series for the average value of AOD for the desert regions. All GLDAS datasets are based on SMOS local overpass time.

First, the AOD data might not have been observed using the deep blue algorithms, mostly because of cloud masking. The visible bands 3 (459 to 479 nm) and 8 (405 to 420 nm) cannot pass through clouds, preventing the use of these data [33]. However, in high cloud coverage season we can still predict the data with a microwave-based SM model. Second, most of the dust particles were likely blown away before observation

by MODIS because the SMOS-MA in box (a)-1 was predicted 7.5 h before MODIS overpassed those areas. This is supported by the fact that particles in box (c)-1 were mostly masked out, as shown in box (b)-1, because they had high AE values, which means that most of the aerosols in box (c)-1 would have been susceptible to being blown away. Boxes (a)-2, (b)-2, and (c)-2 indicate the limitation of MA datasets because
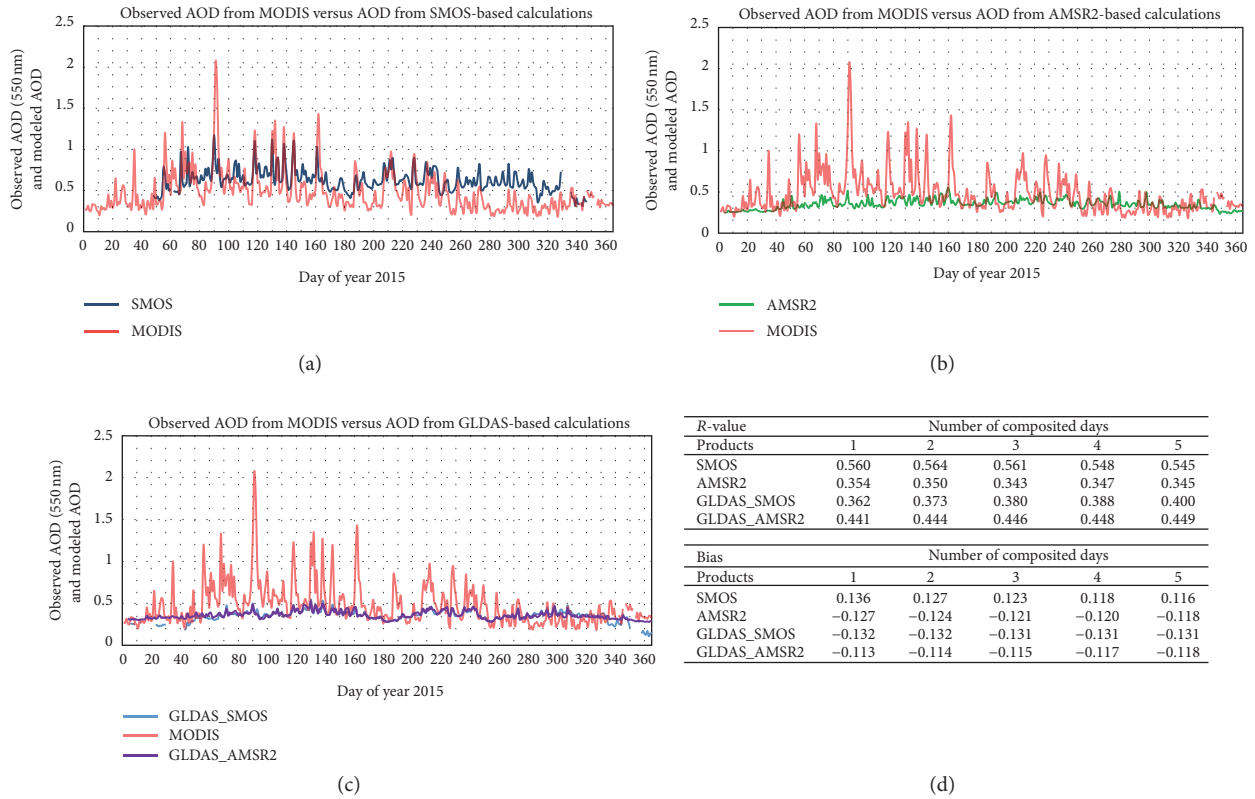
(a)

(b)

(c)

R-value	Number of composited days				
Products	1	2	3	4	5
SMOS	0.560	0.564	0.561	0.548	0.545
AMSR2	0.354	0.350	0.343	0.347	0.345
GLDAS_SMOS	0.362	0.373	0.380	0.388	0.400
GLDAS_AMSR2	0.441	0.444	0.446	0.448	0.449

Bias	Number of composited days				
Products	1	2	3	4	5
SMOS	0.136	0.127	0.123	0.118	0.116
AMSR2	−0.127	−0.124	−0.121	−0.120	−0.118
GLDAS_SMOS	−0.132	−0.132	−0.131	−0.131	−0.131
GLDAS_AMSR2	−0.113	−0.114	−0.115	−0.117	−0.118

(d)

FIGURE 5: Temporal pattern of observed AOD from MODIS and modeled AOD (exponential model based on SMOS, AMSR2, and GLDAS soil moisture and GLDAS wind speed product) for the year 2015. (a) Observed AOD versus modeled AOD based on SMOS soil moisture, (b) observed AOD versus modeled AOD based on AMSR2 soil moisture model, (c) observed AOD versus modeled AOD based on GLDAS soil moisture products after matching UTC time with local times of SMOS and AMSR2, and (d) statistical comparison of 1~5 days composite soil moisture models AOD with observed AOD from MODIS.

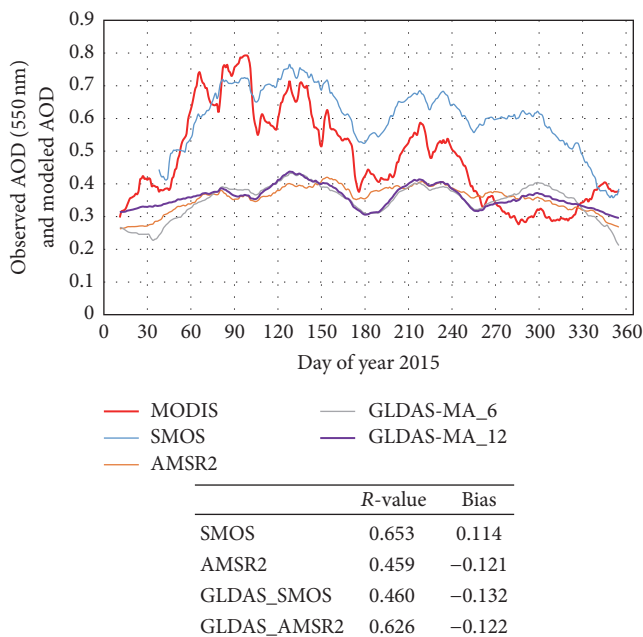|	R-value	Bias
SMOS	0.653	0.114
AMSR2	0.459	−0.121
GLDAS_SMOS	0.460	−0.132
GLDAS_AMSR2	0.626	−0.122

FIGURE 6: 11-day moving average of observed and modeled AOD in different season of the year 2015 with statistical table of correlation coefficient and bias values of AOD model with observed AOD from MODIS.

they can only possibly calculate AOD values over desert areas; thus, MAs are unable to estimate aerosols in nondesert regions. In addition, the MA concept is unreasonable to account for anthropogenic aerosols that were developed from urban areas such as Beijing, China (boxes of (a)-2, (b)-2, and (c)-2), and Seoul, South Korea ((a)-4, (b)-4, and (c)-4).

4.4. Spatial Analysis of MA and AOD from MODIS. We explored the spatial patterns of seasonally averaged AOD calculated from MAs and MODIS-AOD (Figure 8). Generally, the SMOS-MA simulates AOD well in the Taklimakan, Badain Jaran, Tengger, Ulan Buh, and Hobq Deserts; however, it overestimates in the Gurbantunggut, Hunshandake, and Horqin Deserts (Figure 1). Moreover, the prediction in the spring season occurs more frequently than the summer and the fall season. The observed AOD in the fall season is mostly missing in a large portion of the Taklimakan and Gurbantunggut Deserts. This might be due to many rainy days (i.e., monsoon season in the fall) during which clouds could obstruct the MODIS measurements. The AMSR2-MA underestimated the AOD in most of the study regions but captures AOD well in the Gurbantunggut and Gobi Desert regions. Nonetheless, the AMSR2-MA overestimated the AOD in the region (40–45°N and 90–100°E), which may
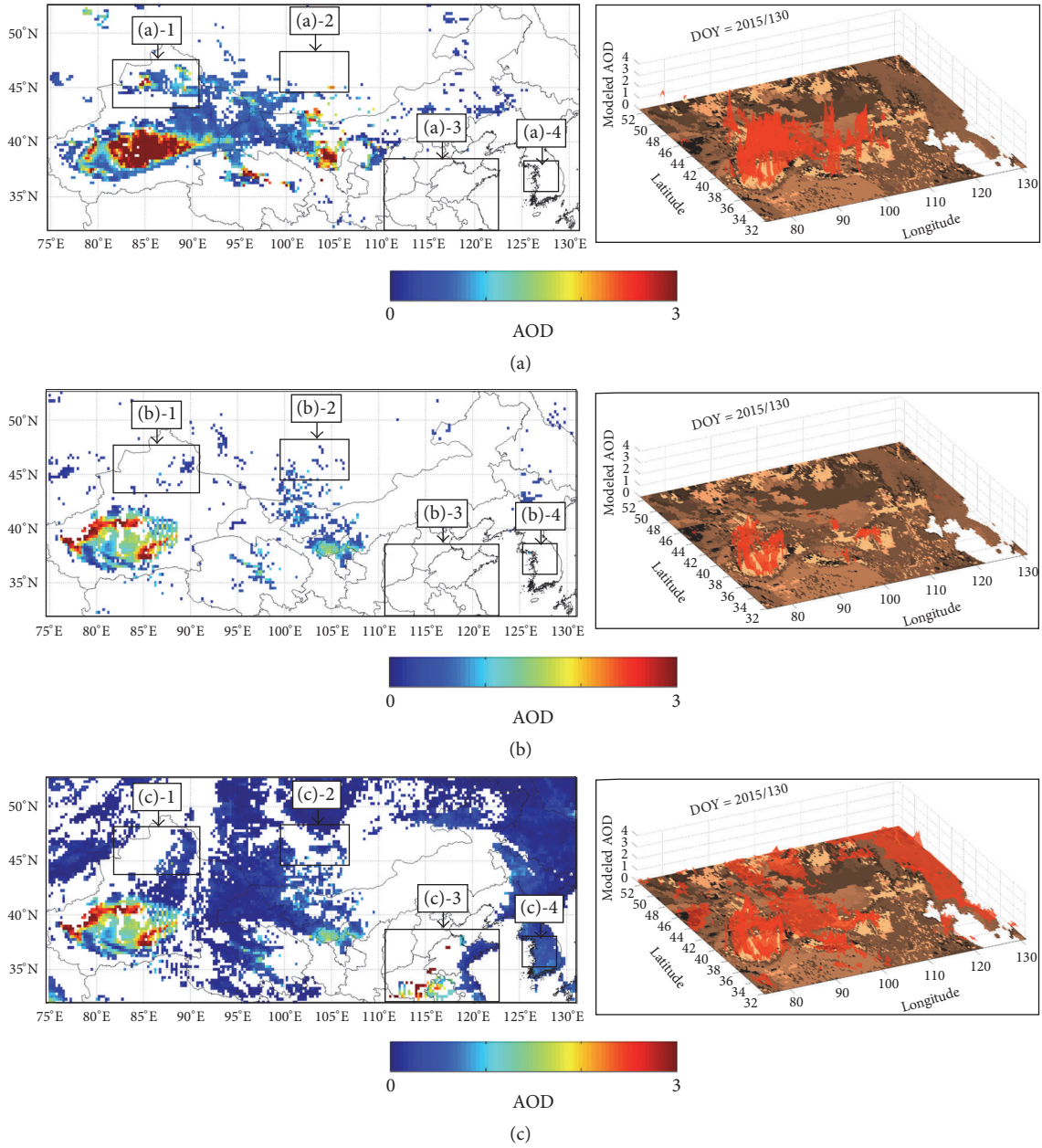
Figure 7: Spatial distribution of AOD in the desert regions of East Asia in day of year 130 in 2015. (a) Modeled AOD based on SMOS soil moisture and GLDAS wind speed, (b) MODIS AOD with Angstrom exponent mask (AE > 0.35, blown dust), and (c) observed AOD from MODIS without Angstrom exponent mask. Images in right column indicate its left side's 3D values, respectively.

be a result of the underestimation of SM, as the model is calculated by SM. Similarly, the GLDAS-MA also captures the AOD well but underestimates it in most of the study areas. The SMOS-MA map clearly determines severe dust source regions, such as the Taklimakan Desert, Badain Jaran Desert, and Hushandake Desert, and Horqin Desert. These regions are also highly related to sources of traveling dust under the prevailing westerlies. Particularly in northeast Asia, Asian dust storms during the most hazardous period might be generated from these areas. These results are consistent with those from numerous prior studies [60, 87, 88], and these are the first time to be identified using only remotely sensed

SM analysis. Other areas that have been known to be dust source regions, such as the Gobi Desert (box 7 in Figure 1), are not included in this study because the sand fraction in that region is low, and the main factors contributing to dust emission in that region are dependent not only on SM and WS but also on vegetation conditions (e.g., dead leaves and NDVI variation) [15, 89]. In future studies, the SM contents retrieved with other satellite-based sensors (i.e., ASCAT and SMAP) and the corresponding land properties will be considered for specific land surface conditions (i.e., vegetated areas) and other factors (i.e., NDVI and clay and silt fraction) in dynamic environments.
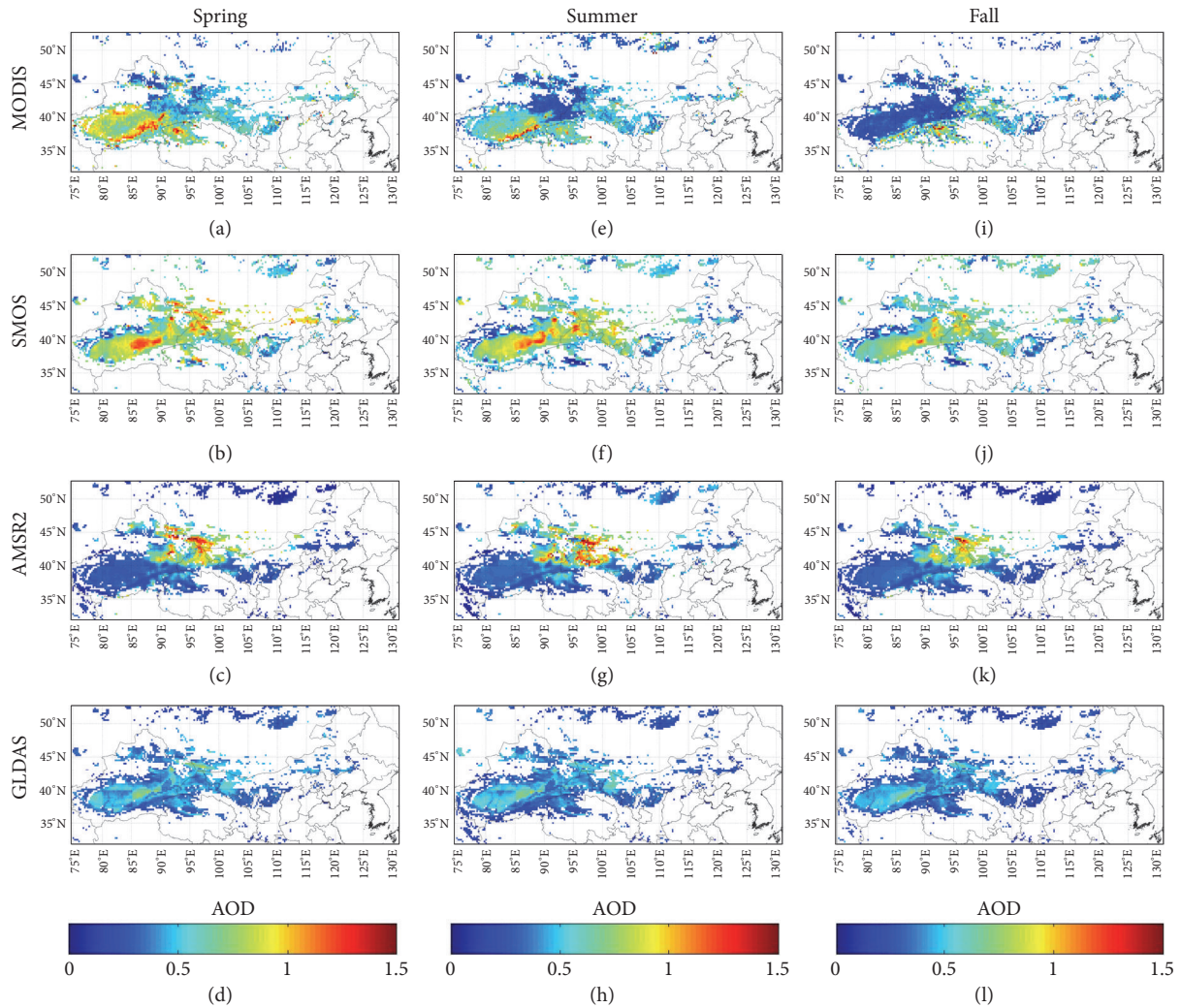
FIGURE 8: Spatial distribution of seasonal mean for observed and modeled AOD in the desert regions of East Asia.

5. Summary and Conclusions

In this study, SMOS, AMSR2, and GLDAS/Noah SM products in combination with GLDAS WS product were used to predict the AOD in 2015 over East Asian desert areas. SMOS-MA better estimated the AOD compared to the AMSR2-MA and GLDAS-MA in desert regions with highly polluted atmospheric conditions. The aerosol products, observed from the MODIS sensor, were used as a reference dataset to validate the MA. The validation results showed that the SMOS-MA captured the temporal patterns well, with a R-value 0.56; however, it overestimated the reference AOD. A short-term trend analysis was conducted by calculating the 11-day moving average of MAs, the result of which showed that the SMOS-MA dataset demonstrated superior performance in capturing the short-term trends when compared to other MAs ($R = 0.65$). In addition, the results from investigating the impact of the antecedent SM on dust outbreaks showed that R-values have not changed much with respect to different antecedent SM conditions. In this regard, we assume that the

antecedent SM condition could not be the major factor that governs the timing of dust outbreaks. This is supported by the fact that bare desert regions have persistently very low SM conditions so that the WS, which fluctuates relatively more severely than SM (Figures 4(b) and 4(d)) over desert regions, would play a more pivotal role in triggering dust outbreaks. Moreover, spatial maps in different seasons also demonstrated that the SMOS-MA showed better consistency with the reference dataset compared to other MAs. The findings of this study reveal the application of microwave-based SM retrievals for near-real time dust outbreak predictions and short-term dust outbreak trend analysis. Future research will focus on the most robust modeling approach, based on machine learning, to improve MA products by utilizing the most recent and accurate available SM dataset from SMAP. In addition, Essential Climate Variable SM datasets are considered to be strong candidate products for the long-term AOD trend analysis, and the Representative Concentration Pathways dataset may be utilized to investigate AOD trends in the near future.

Competing Interests

Acknowledgments

References

[1] N. M. Mahowald, D. R. Muhs, S. Levis et al., "Change in atmospheric mineral aerosols in response to climate: last glacial period, preindustrial, modern, and doubled carbon dioxide climates," *Journal of Geophysical Research Atmospheres*, vol. 111, no. D10, Article ID D10202, 2006.

[2] R. L. Miller and I. Tegen, "Climate response to soil dust aerosols," *Journal of Climate*, vol. 11, no. 12, pp. 3247–3267, 1998.

[3] I. N. Sokolik and O. B. Toon, "Direct radiative forcing by anthropogenic airborne mineral aerosols," *Nature*, vol. 381, no. 6584, pp. 681–683, 1996.

[4] I. Tegen, A. A. Lacis, and I. Fung, "The influence on climate forcing of mineral aerosols from disturbed soils," *Nature*, vol. 380, no. 6573, pp. 419–422, 1996.

[5] S. Wurzler, T. G. Reisin, and Z. Levin, "Modification of mineral dust particles by cloud processing and subsequent effects on drop size distributions," *Journal of Geophysical Research Atmospheres*, vol. 105, no. 4, pp. 4501–4512, 2000.

[6] Z. Levin, E. Ganor, and V. Gladstein, "The effects of desert particles coated with sulfate on rain formation in the eastern Mediterranean," *Journal of Applied Meteorology*, vol. 35, no. 9, pp. 1511–1523, 1996.

[7] G. S. Okin, N. Mahowald, O. A. Chadwick, and P. Artaxo, "Impact of desert dust on the biogeochemistry of phosphorus in terrestrial ecosystems," *Global Biogeochemical Cycles*, vol. 18, no. 2, 2004.

[8] T. Larssen and G. R. Carmichael, "Acid rain and acidification in China: the importance of base cation deposition," *Environmental Pollution*, vol. 110, no. 1, pp. 89–102, 2000.

[9] P. G. Falkowski, R. T. Barber, and V. Smetacek, "Biogeochemical controls and feedbacks on ocean primary production," *Science*, vol. 281, no. 5374, pp. 200–206, 1998.

[10] S. P. Parajuli, Z. Yang, and G. Kocurek, "Mapping erodibility in dust source regions based on geomorphology, meteorology, and remote sensing," *Journal of Geophysical Research: Earth Surface*, vol. 119, no. 9, pp. 1977–1994, 2014.

[11] H. Breitkreuz, M. Schroedter-Homscheidt, and T. Holzer-Popp, "A case study to prepare for the utilization of aerosol forecasts in solar energy industries," *Solar Energy*, vol. 81, no. 11, pp. 1377–1385, 2007.

[12] J. M. Prospero, P. Ginoux, O. Torres, S. E. Nicholson, and T. E. Gill, "Environmental characterization of global sources of atmospheric soil dust identified with the Nimbus 7 Total Ozone Mapping Spectrometer (TOMS) absorbing aerosol product," *Reviews of Geophysics*, vol. 40, no. 1, pp. 1–31, 2002.

[13] H. Lee, Y. Honda, Y.-H. Lim, Y. L. Guo, M. Hashizume, and H. Kim, "Effect of Asian dust storms on mortality in three Asian cities," *Atmospheric Environment*, vol. 89, pp. 309–317, 2014.

[14] H.-J. Kwon, S.-H. Cho, Y. Chun, F. Lagarde, and G. Pershagen, "Effects of the Asian dust events on daily mortality in Seoul, Korea," *Environmental Research*, vol. 90, no. 1, pp. 1–5, 2002.

[15] Y. Kurosaki, M. Shinoda, and M. Mikami, "What caused a recent increase in dust outbreaks over East Asia?" *Geophysical Research Letters*, vol. 38, no. 11, Article ID L11702, 2011.

[16] Y. Kurosaki and M. Mikami, "Recent frequent dust events and their relation to surface wind in East Asia," *Geophysical Research Letters*, vol. 30, no. 14, 2003.

[17] M. Ishizuka, M. Mikami, Y. Yamada, F. Zeng, and W. Gao, "An observational study of soil moisture effects on wind erosion at a gobi site in the Taklimakan Desert," *Journal of Geophysical Research: Atmospheres*, vol. 110, no. 15, 2005.

[18] S. Ravi and P. D'Odorico, "A field-scale analysis of the dependence of wind erosion threshold velocity on air humidity," *Geophysical Research Letters*, vol. 32, no. 21, pp. 1–4, 2005.

[19] S. Ravi, P. D'Odorico, T. M. Over, and T. M. Zobeck, "On the effect of air humidity on soil susceptibility to wind erosion: the case of air-dry soils," *Geophysical Research Letters*, vol. 31, no. 9, 2004.

[20] O. Chomette, M. Legrand, and B. Marticorena, "Determination of the wind speed threshold for the emission of desert dust using satellite remote sensing in the thermal infrared," *Journal of Geophysical Research: Atmospheres*, vol. 104, no. 24, pp. 31207–31215, 1999.

[21] D. W. Fryrear, "Soil cover and wind erosion," *Transactions of the American Society of Agricultural Engineers*, vol. 28, no. 3, pp. 781–784, 1985.

[22] C. McKenna-Neuman and W. G. Nickling, "A theoretical and wind tunnel investigation of the effect of capillary water on the entrainment of sediment by wind," *Canadian Journal of Soil Science*, vol. 69, no. 1, pp. 79–96, 1989.

[23] P. Y. Belly, *Sand Movement by Wind*, USACE, 1964.

[24] H. Kim and M. Choi, "Impact of soil moisture on dust outbreaks in East Asia: using satellite and assimilation data," *Geophysical Research Letters*, vol. 42, no. 8, pp. 2789–2796, 2015.

[25] K. Schepanski, I. Tegen, and A. Macke, "Comparison of satellite based observations of Saharan dust source areas," *Remote Sensing of Environment*, vol. 123, pp. 90–97, 2012.

[26] H. Cao, F. Amiraslani, J. Liu, and N. Zhou, "Identification of dust storm source areas in West Asia using multiple environmental datasets," *Science of the Total Environment*, vol. 502, pp. 224–235, 2015.

[27] S. S. Park, J. Kim, J. Lee et al., "Combined dust detection algorithm by using MODIS infrared channels over East Asia," *Remote Sensing of Environment*, vol. 141, pp. 24–39, 2014.

[28] S. A. Christopher, P. Gupta, B. Johnson, C. Ansell, H. Brindley, and J. Haywood, "multi-sensor satellite remote sensing of dust aerosols over north africa during gerbils," *Quarterly Journal of the Royal Meteorological Society*, vol. 137, no. 658, pp. 1168–1178, 2011.

[29] M. C. Baddock, J. E. Bullard, and R. G. Bryant, "Dust source identification using MODIS: a comparison of techniques applied to the Lake Eyre Basin, Australia," *Remote Sensing of Environment*, vol. 113, no. 7, pp. 1511–1528, 2009.

[30] R. A. Hansell, S. C. Ou, K. N. Liou et al., "Simultaneous detection/separation of mineral dust and cirrus clouds using MODIS thermal infrared window data," *Geophysical Research Letters*, vol. 34, no. 11, Article ID L11808, 2007.

[31] K. Schepanski, I. Tegen, B. Laurent, B. Heinold, and A. Macke, "A new Saharan dust source activation frequency map derived from MSG-SEVIRI IR-channels," *Geophysical Research Letters*, vol. 34, no. 18, Article ID L18803, 2007.

[32] J. K. Roskovensky and K. N. Liou, "Differentiating airborne dust from cirrus clouds using MODIS data," *Geophysical Research Letters*, vol. 32, no. 12, pp. 1–5, 2005.

[33] N. C. Hsu, S.-C. Tsay, M. D. King, and J. R. Herman, "Aerosol properties over bright-reflecting source regions," *IEEE Transactions on Geoscience and Remote Sensing*, vol. 42, no. 3, pp. 557–569, 2004.

[34] S. D. Miller, "A consolidated technique for enhancing desert dust storms with MODIS," *Geophysical Research Letters*, vol. 30, no. 20, 2003.

[35] T. J. Jackson, M. H. Cosh, R. Bindlish et al., "Validation of advanced microwave scanning radiometer soil moisture products," *IEEE Transactions on Geoscience and Remote Sensing*, vol. 48, no. 12, pp. 4256–4272, 2010.

[36] Y. H. Kerr, P. Waldteufel, J.-P. Wigneron et al., "The SMOS mission: new tool for monitoring key elements ofthe global water cycle," *Proceedings of the IEEE*, vol. 98, no. 5, pp. 666–687, 2010.

[37] M. Choi and J. M. Jacobs, "Temporal variability corrections for Advanced Microwave Scanning Radiometer E (AMSR-E) surface soil moisture: case study in Little River Region, Georgia, U.S," *Sensors*, vol. 8, no. 4, pp. 2617–2627, 2008.

[38] Y. H. Kerr, P. Waldteufel, P. Richaume et al., "The SMOS soil moisture retrieval algorithm," *IEEE Transactions on Geoscience and Remote Sensing*, vol. 50, no. 5, pp. 1384–1403, 2012.

[39] W. Wagner, G. Lemoine, and H. Rott, "A method for estimating soil moisture from ERS Scatterometer and soil data," *Remote Sensing of Environment*, vol. 70, no. 2, pp. 191–207, 1999.

[40] D. J. Leroux, Y. H. Kerr, P. Richaume, and R. Fieuzal, "Spatial distribution and possible sources of SMOS errors at the global scale," *Remote Sensing of Environment*, vol. 133, pp. 240–250, 2013.

[41] R. M. Parinussa, G. Wang, T. R. H. Holmes et al., "Global surface soil moisture from the Microwave Radiation Imager onboard the Fengyun-3B satellite," *International Journal of Remote Sensing*, vol. 35, no. 19, pp. 7007–7029, 2014.

[42] C.-H. Su, D. Ryu, R. I. Young, A. W. Western, and W. Wagner, "Inter-comparison of microwave satellite soil moisture retrievals over the Murrumbidgee Basin, southeast Australia," *Remote Sensing of Environment*, vol. 134, pp. 1–11, 2013.

[43] W. Wagner, S. Hahn, R. Kidd et al., "The ASCAT soil moisture product: a review of its specifications, validation results, and emerging applications," *Meteorologische Zeitschrift*, vol. 22, no. 1, pp. 5–33, 2013.

[44] L. Brocca, S. Hasenauer, T. Lacava et al., "Soil moisture estimation through ASCAT and AMSR-E sensors: an intercomparison and validation study across Europe," *Remote Sensing of Environment*, vol. 115, no. 12, pp. 3390–3408, 2011.

[45] W. A. Dorigo, K. Scipal, R. M. Parinussa et al., "Error characterisation of global active and passive microwave soil moisture datasets," *Hydrology and Earth System Sciences*, vol. 14, no. 12, pp. 2605–2616, 2010.

[46] S. Kim, Y. Y. Liu, F. M. Johnson, R. M. Parinussa, and A. Sharma, "A global comparison of alternate AMSR2 soil moisture products: why do they differ?" *Remote Sensing of Environment*, vol. 161, pp. 43–62, 2015.

[47] E. Cho, C.-H. Su, D. Ryu, H. Kim, and M. Choi, "Does AMSR2 produce better soil moisture retrievals than AMSR-E over Australia?" *Remote Sensing of Environment*, vol. 188, pp. 95–105, 2017.

[48] Z. Bartalis, W. Wagner, V. Naeimi et al., "Initial soil moisture retrievals from the METOP-A Advanced Scatterometer (ASCAT)," *Geophysical Research Letters*, vol. 34, no. 20, Article ID L20401, 2007.

[49] W. A. Dorigo, A. Gruber, R. A. M. De Jeu et al., "Evaluation of the ESA CCI soil moisture product using ground-based observations," *Remote Sensing of Environment*, vol. 162, pp. 380–395, 2015.

[50] D. Ryu, T. J. Jackson, R. Bindlish, and D. M. Le Vine, "L-band microwave observations over land surface using a two-dimensional synthetic aperture radiometer," *Geophysical Research Letters*, vol. 34, no. 14, 2007.

[51] C. Rüdiger, J. P. Walker, Y. H. Kerr et al., "Toward vicarious calibration of microwave remote-sensing satellites in arid environments," *IEEE Transactions on Geoscience and Remote Sensing*, vol. 52, no. 3, pp. 1749–1760, 2014.

[52] E. Cho, H. Moon, and M. Choi, "First assessment of the Advanced Microwave Scanning Radiometer 2 (AMSR2) soil moisture contents in Northeast Asia," *Journal of the Meteorological Society of Japan*, vol. 93, no. 1, pp. 117–129, 2015.

[53] Q. Wu, H. Liu, L. Wang, and C. Deng, "Evaluation of AMSR2 soil moisture products over the contiguous United States using in situ data from the international soil moisture network," *International Journal of Applied Earth Observation and Geoinformation*, vol. 45, pp. 187–199, 2016.

[54] R. E. Dickinson, A. Henderson-Sellers, P. J. Kennedy, and M. F. Wilson, "Biosphere-Atmosphere Transfer Scheme (BATS) for the NCAR community climate model," NCAR Technical Note NCAR/TN-275+STR, NCAR, Boulder, Colo, USA, 1986.

[55] J. S. Olson, *Global Ecosystems Framework: Definitions. Internal Report*, vol. 37, USGS EROS Data Center, Sioux Falls, SD, USA, 1994.

[56] FAO/IIASA/ISRIC/ISSCAS/JRC, *Harmonized World Soil Database (Version 1.2)*, FAO, Rome, Italy; IIASA, Laxenburg, Austria, 2012.

[57] A. Fadil, H. Rhinane, A. Kaoukaya, Y. Kharchaf, and O. A. Bachir, "Hydrologic modeling of the bouregreg watershed (Morocco) using GIS and SWAT model," *Journal of Geographic Information System*, vol. 3, no. 4, pp. 279–289, 2011.

[58] N. H. Batjes, "Harmonized soil profile data for applications at global and continental scales: updates to the WISE database," *Soil Use and Management*, vol. 25, no. 2, pp. 124–127, 2009.

[59] K. E. Saxton and W. J. Rawls, "Soil water characteristic estimates by texture and organic matter for hydrologic solutions," *Soil Science Society of America Journal*, vol. 70, no. 5, pp. 1569–1578, 2006.

[60] J. Huang, J. Ge, and F. Weng, "Detection of Asia dust storms using multisensor satellite measurements," *Remote Sensing of Environment*, vol. 110, no. 2, pp. 186–191, 2007.

[61] J. Sun, M. Zhang, and T. Liu, "Spatial and temporal characteristics of dust storms in China and its surrounding regions, 1960–1999: Relations to source area and climate," *Journal of Geophysical Research Atmospheres*, vol. 106, no. D10, Article ID 2000JD900665, pp. 10325–10333, 2001.

[62] X. Wang, Z. Dong, J. Zhang, and L. Liu, "Modern dust storms in China: an overview," *Journal of Arid Environments*, vol. 58, no. 4, pp. 559–574, 2004.

[63] H. Lee, H. Kim, Y. Honda, Y.-H. Lim, and S. Yi, "Effect of Asian dust storms on daily mortality in seven metropolitan cities of Korea," *Atmospheric Environment*, vol. 79, pp. 510–517, 2013.

[64] Y. Kurosaki and M. Mikami, "Threshold wind speed for dust emission in east Asia and its seasonal variations," *Journal of Geophysical Research Atmospheres*, vol. 112, no. 17, Article ID D17202, 2007.

[65] T. Lacava, P. Matgen, L. Brocca et al., "A first assessment of the SMOS soil moisture product with in situ and modeled data in Italy and Luxembourg," *IEEE Transactions on Geoscience and Remote Sensing*, vol. 50, no. 5, pp. 1612–1622, 2012.

[66] C. Albergel, P. de Rosnay, C. Gruhier et al., "Evaluation of remotely sensed and modelled soil moisture products using global ground-based in situ observations," *Remote Sensing of Environment*, vol. 118, pp. 215–226, 2012.

[67] R. A. M. De Jeu, W. Wagner, T. R. H. Holmes, A. J. Dolman, N. C. Van De Giesen, and J. Friesen, "Global soil moisture patterns observed by space borne microwave radiometers and scatterometers," *Surveys in Geophysics*, vol. 29, no. 4-5, pp. 399–420, 2008.

[68] R. Oliva, E. Daganzo-Eusebio, Y. H. Kerr et al., "SMOS radio frequency interference scenario: status and actions taken to improve the RFI environment in the 1400–1427-MHZ passive band," *IEEE Transactions on Geoscience and Remote Sensing*, vol. 50, no. 5, pp. 1427–1439, 2012.

[69] T. Mo, B. J. Choudhury, T. J. Schmugge, J. R. Wang, and T. J. Jackson, "A model for microwave emission from vegetation-covered fields," *Journal of Geophysical Research*, vol. 87, no. 13, pp. 11229–11237, 1982.

[70] R. M. Parinussa, T. R. H. Holmes, M. T. Yilmaz, and W. T. Crow, "The impact of land surface temperature on soil moisture anomaly detection from passive microwave observations," *Hydrology and Earth System Sciences*, vol. 15, no. 10, pp. 3135–3151, 2011.

[71] L. A. Remer, Y. J. Kaufman, D. Tanré et al., "The MODIS aerosol algorithm, products, and validation," *Journal of the Atmospheric Sciences*, vol. 62, no. 4, pp. 947–973, 2005.

[72] A. Savtchenko, D. Ouzounov, S. Ahmad et al., "Terra and Aqua MODIS products available from NASA GES DAAC," *Advances in Space Research*, vol. 34, no. 4, pp. 710–714, 2004.

[73] M. Sorek-Hamer, I. Kloog, P. Koutrakis et al., "Assessment of PM2.5 concentrations over bright surfaces using MODIS satellite observations," *Remote Sensing of Environment*, vol. 163, pp. 180–185, 2015.

[74] P. Ginoux, J. M. Prospero, T. E. Gill, N. C. Hsu, and M. Zhao, "Global-scale attribution of anthropogenic and natural dust sources and their emission rates based on MODIS Deep Blue aerosol products," *Reviews of Geophysics*, vol. 50, no. 3, 2012.

[75] M. Decker, M. A. Brunke, Z. Wang, K. Sakaguchi, X. Zeng, and M. G. Bosilovich, "Evaluation of the reanalysis products from GSFC, NCEP, and ECMWF using flux tower observations," *Journal of Climate*, vol. 25, no. 6, pp. 1916–1944, 2012.

[76] J. Sheffield, G. Goteti, and E. F. Wood, "Development of a 50-year high-resolution global dataset of meteorological forcings for land surface modeling," *Journal of Climate*, vol. 19, no. 13, pp. 3088–3111, 2006.

[77] M. Rodell, P. R. Houser, U. Jambor et al., "The global land data assimilation system," *Bulletin of the American Meteorological Society*, vol. 85, no. 3, pp. 381–394, 2004.

[78] H. Seyyedi, E. N. Anagnostou, E. Beighley, and J. McCollum, "Satellite-driven downscaling of global reanalysis precipitation products for hydrological applications," *Hydrology and Earth System Sciences*, vol. 18, no. 12, pp. 5077–5091, 2014.

[79] K. E. Mitchell, D. Lohmann, P. R. Houser et al., "The multi-institution North American Land Data Assimilation System (NLDAS): utilizing multiple GCIP products and partners in a continental distributed hydrological modeling system," *Journal of Geophysical Research D: Atmospheres*, vol. 109, no. D7, 2004.

[80] T. F. Eck, B. N. Holben, J. S. Reid et al., "Wavelength dependence of the optical depth of biomass burning, urban, and desert dust aerosols," *Journal of Geophysical Research Atmospheres*, vol. 104, no. 24, pp. 31333–31349, 1999.

[81] Z. Dong, X. Liu, and X. Wang, "Wind initiation thresholds of the moistened sands," *Geophysical Research Letters*, vol. 29, no. 12, pp. 25-1–25-4, 2002.

[82] F. Fécan, B. Marticorena, and G. Bergametti, "Parametrization of the increase of the aeolian erosion threshold wind friction velocity due to soil moisture for arid and semi-arid areas," *Annales Geophysicae*, vol. 17, no. 1, pp. 149–157, 1999.

[83] D. G. Waggoner and I. N. Sokolik, "Seasonal dynamics and regional features of MODIS-derived land surface characteristics in dust source regions of East Asia," *Remote Sensing of Environment*, vol. 114, no. 10, pp. 2126–2136, 2010.

[84] D. A. Gillette, J. Adams, D. Muhs, and R. Kihl, "Threshold friction velocities and rupture moduli for crusted desert soils for the input of soil particles into the air," *Journal of Geophysical Research*, vol. 87, no. 11, pp. 9003–9015, 1982.

[85] R. D. Koster and M. J. Suarez, "Soil moisture memory in climate models," *Journal of Hydrometeorology*, vol. 2, no. 6, pp. 558–570, 2001.

[86] S. I. Seneviratne and R. D. Koster, "A revised framework for analyzing soil moisture memory in climate data: derivation and interpretation," *Journal of Hydrometeorology*, vol. 13, no. 1, pp. 404–412, 2012.

[87] A. Higurashi and T. Nakajima, "Detection of aerosol types over the East China Sea near Japan from four-channel satellite data," *Geophysical Research Letters*, vol. 29, no. 17, pp. 17-1–17-4, 2002.

[88] J. M. Haywood, V. Ramaswamy, and B. J. Soden, "Tropospheric aerosol climate forcing in clear-sky satellite observations over the oceans," *Science*, vol. 283, no. 5406, pp. 1299–1303, 1999.

[89] X. Liu, Z.-Y. Yin, X. Zhang, and X. Yang, "Analyses of the spring dust storm frequency of northern China in relation to antecedent and concurrent wind, precipitation, vegetation, and soil moisture conditions," *Journal of Geophysical Research: Atmospheres*, vol. 109, no. 16, 2004.

Journal of
Geochemistry

Scientifica

International Journal of
Ecology

The Scientific
World Journal

Journal of
Mining

Journal of
Earthquakes

Paleontology Journal

Journal of
Petroleum Engineering
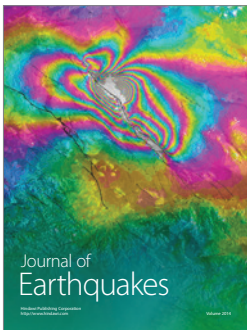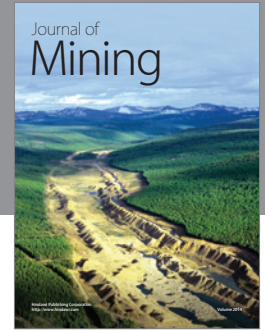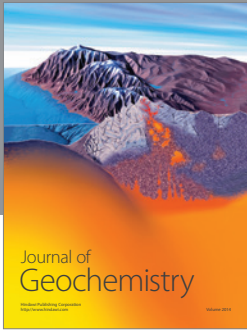
Submit your manuscripts at
https://www.hindawi.com

Hindawi

International Journal of
Geophysics

Advances in
Meteorology

Journal of
Climatology

Advances in
Geology

Advances in
Oceanography

International Journal of
Oceanography

International Journal of
Mineralogy

Journal of
Geological Research

International Journal of
Atmospheric Sciences

Applied &
Environmental
Soil Science

Journal of
Computational
Environmental Sciences